Chinese Journal of Structural Chemistry

REVIEW

Recent Progress in π-Conjugated Polymer-Inorganic Heterostructures for Photocatalysis

Yu-Qin Xing[1] and Shi-Yong Liu[1]*

[1]*Jiangxi Provincial Key Laboratory of Functional Molecular Materials Chemistry, Jiangxi University of Science and Technology, Ganzhou 341000, China*

ABSTRACT Polymer-inorganic (P-I) soft-hard heterostructures & heterojunction photocatalysts, featured by large interfacial contact, efficient charge separation, broad light absorption and maximized redox capacity, have received great attention for their applications in energy conversion and environmental remediation. In this minireview, the classification and mechanism of P-I heterojunctions, *i.e.*, type-I/II, p-n, Z-scheme and S-scheme heterojunctions, and their preparation methods are firstly introduced. Next, the photocatalytic applications of P-I heterojunctions, including water splitting, environmental remediation and carbon dioxide reduction, are extensively reviewed. Lastly, a brief summary and perspectives on ongoing challenges and opportunities to construct high performance P-I soft-hard photocatalysts are intensively highlighted. We envision this review will provide a picture of the state-of-the-art achievements and promote the photocatalytic applications of P-I heterostructures in energy conversion and environmental remediation.

Keywords: polymer-inorganic hybrid, heterojunction, photocatalytic water splitting, photocatalytic CO_2 reduction, photocatalytic environmental remediation

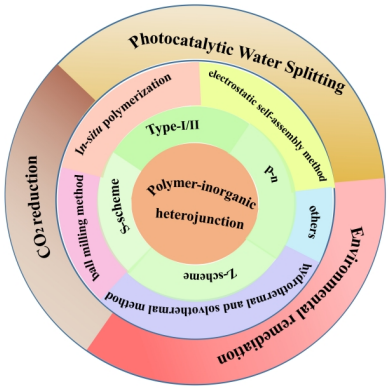

n INTRODUNTION

The ever-increasing consumption of traditional fossil fuel has led to severe energy and environmental crisis. Carbon dioxide (CO_2), sulfur dioxide (SO_2) and other harmful gases released by the combustion of fossil fuels bring about the greenhouse effect, acid rain and many other environmental problems.[1-3] Thus, it is highly urgent to develop sustainable and renewable energies to solve environmental problems. Semiconductor photocatalysis technology has arisen tremendous attention because of its great potential *via* direct utilization of the inexhaustible and renewable solar energy to solve both energy and environmental problems. Photocatalysis can easily convert solar energy into storable chemical energy. Photocatalytic H_2O splitting into H_2 and O_2, conversion of CO_2 to hydrocarbons (*e.g.*, CH_4) and fuels (*e.g.*, CH_3OH, C_2H_5OH and HCOOH) and environmental remediation are three major applications (Figure 1) that have attracted extensive attention.[4,5] Typically, photocatalytic reactions include four steps (Figure 1): (i) formation of photogenerated e^- - h^+ pairs upon light absorption ($hv \geq E_g$); (ii) separation of electron-hole pairs; (iii) charge migration to the photocatalyst surface; and (iv) electrons/holes participating in reduction/oxidation reactions. Thereby, a rational design of photocatalysts and reaction system should simultaneously take these four factors into account.

Since TiO_2 was discovered for the photoelectrochemical splitting water to generate hydrogen (H_2) by Fujishima et al in 1972,[6] numerous inorganic semiconductor photocatalysts have been explored. According to the energy bands and redox capacities (Figure 2), inorganic photocatalysts can be typically divided into oxidation photocatalysts (TiO_2, ZnO, WO_3, α-Fe_2O_3, $BiVO_4$ and Cu_2O, etc.), reduction photocatalysts (CdS, Cu_2O, C_3N_4, etc.) and metal sulfide photocatalysts (CdS, ZnS, MoS_2, etc.). Generally speaking, oxidation and reduction semiconductors are respectively featured by lower valence band (VB) and higher conduction band (CB), which accordingly benefit photocatalytic oxidative reactions (e.g., water oxidation half reaction) and reductive reaction (e.g., water reduction half reaction), respectively. Meanwhile, metal sulfides possess VBs and CBs that fall between those of oxidation and reduction semiconductors (Figure 2). Despite remarkable progress which has been made in inorganic-based photocatalysis in the past decades, most of inorganic semiconductors are still far from practical applications owing to their limited light absorption and fast recombination of photogenerated e^- - h^+ pairs.

As counterparts of inorganic semiconductors, organic polymer semiconductor photocatalysts featured by widely adjustable band gap, abundant structural diversity, excellent optical and electronic properties have received widespread attention. Yanagida et al. first reported the conjugated linear poly(p-phenylene) for photocatalytic hydrogen production (PHP) under ultraviolet light.[7] Besides, Wang et al. proposed the new application of polymeric graphitic carbon nitride (g-C_3N_4) featuring simple preparation process and high thermal stability similar to inorganic semiconductors,

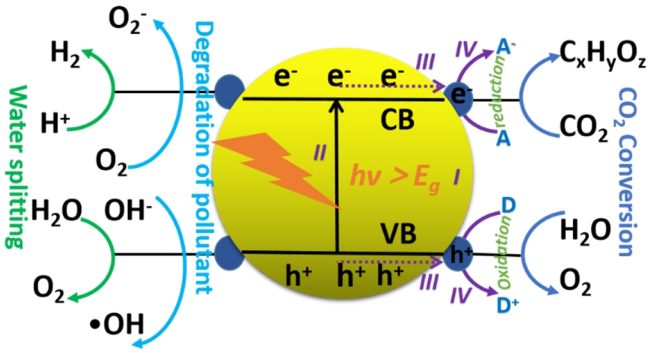

Figure 1. Diagram of the basic pathways of photocatalytic water splitting, pollutant degradation, and CO_2 reduction.

DOI: 10.14102/j.cnki.0254-5861.2022-0188

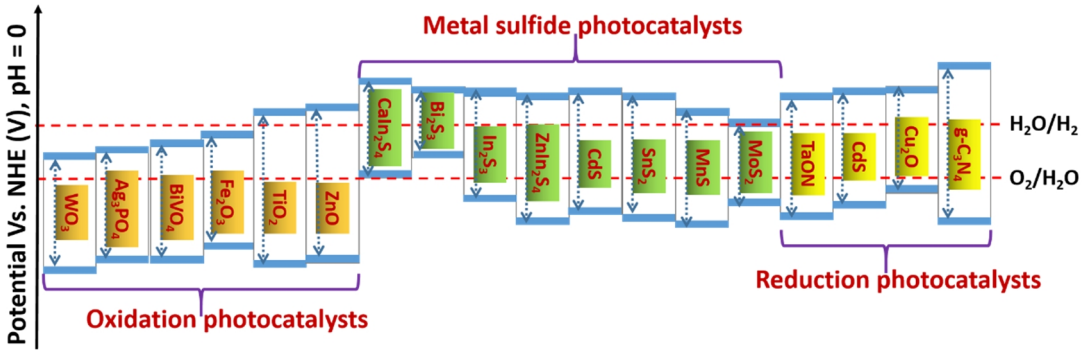

Figure 2. VB and CB alignments of common inorganic photocatalysts.

which shows excellent photocatalytic hydrogen evolution rate (HER) and has become a research hotspot in photocatalysis.[8] Different from rigid g-C_3N_4, conjugated polymers (CPs) synthesized *via* wet chemistry, such as C-C bond cross couplings, have attracted extensive attention due to their large delocalized π-system, widely tunable structures, excellent photoelectrochemical properties, facile optimization of bandgaps, and so on.[9-12] In many cases, they can exhibit strong absorptance in a wide range of light wavelength. However, polymeric semiconductor photocatalysts still suffer from the drawbacks of poor stability and short exciton diffusion length in tens of nanometers. The huge challenge in photocatalysis is that photogenerated electron-hole pairs thermodynamically tend to recombine at the surface/interface attributed to strong Coulombic attraction, which is unfavorable to the photocatalytic redox process. Meanwhile, it is irreconcilable for a single semiconductor photocatalyst which simultaneously possesses narrow bandgap and strong redox ability (Figure 1). Heterojunction appears at this point when simultaneously taking broad light absorption and strong redox ability into account, which can hardly be satisfied by a single semiconductor. Among varied hybridization strategies,[13-15] the most straightforward way is the construction of heterostructures that can integrate advantages of individual components while alleviate respective shortcomings. Till now, heterojunctions for photocatalysis have mainly focused on inorganic-inorganic dual semiconductors.[16,17] Besides, many heterojunctions between g-C_3N_4 and metal oxide semiconductors have also been developed.[18] However, g-C_3N_4, as an n-type semiconductor with wide bandgap and rigid structure, still suffers from disadvantages of poor light absorptance and limited modification of chemical structures. In recent years, the heterojunctions based on inorganic semiconductors and π-conjugated soft polymers with widely tunable optical properties and tailorable structures for varied photocatalytic applications have received great attention.[19,20] Compared to inorganic-inorganic heterojunction, the unique property of P-I heterojunction lies in that its heterojunction can be finely modulated by tunning the ratio of polymer to inorganic semiconductor. On the other hand, compared to polymer-polymer heterojunctions, the P-I soft-hard heterojunctions have the unique properties of higher stability and lower cost. Hence, P-I heterojunctions can combine the advantages of both polymer and inorganic semiconductors and meanwhile overcome their respective shortcomings.

This minireview summarizes the latest progress of P-I soft-hard heterojunctions, including their preparation methods, mechanism study, applications and prospects. According to the pathway of charge transfer, P-I photocatalytic heterojunctions can be mainly classified as I/II type, p-n junction, Z- and S-scheme mechanisms. Meanwhile, the applications of P-I heterojunction photocatalysts mainly focus on three aspects, *i.e.*, photocatalytic hydrogen or oxygen production, CO_2 reduction and degradation of organic pollutants. Besides the previous excellent reviews on the progress of Z- or S-scheme heterojunction photocatalysts,[21,22] a comprehensive and timely review on the P-I heterojunctions for photocatalysis should be quite instructive and necessary.

n TYPES OF P-I PHOTOCATALYTIC HETEROJUNCTIONS AND MECHANISM STUDIES

The construction of heterojunction can facilitate the transport of charge carriers to enhance photocatalytic performance. Appropriate VB and CB are required with matching energy band levels to construct P-I heterojunctions. According to the transfer of photogenerated charge, the heterostructure photocatalysts can be generally divided into following four categories, *i.e.*, I/II type, p-n junction, Z-scheme and S-scheme mechanisms (Figure 3).

Types of P-I Heterojunctions. For type-I heterojunction (Figure 3a), the CB of semiconductor A (SC_A) is higher than that of semiconductor B (SC_B), while the VB of SC_A is lower than that of SC_B. As a result, the electrons and holes are thus accumulated on SC_B

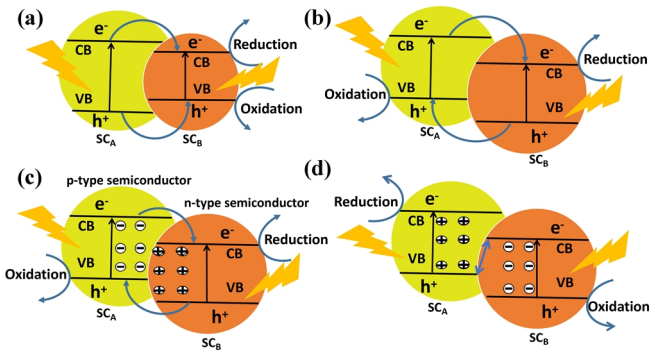

Figure 3. Schematic illustration of charge carrier transfer in (a) type-I, (b) type-II, (c) p-n, (d) Z- or S-scheme heterojunctions (SC_A: semiconductor A; SC_B: semiconductor B).

Chin. J. Struct. Chem. **2022**, 41, 2209056-2209068
DOI: 10.14102/j.cnki.0254-5861.2022-0188

and SC_A, respectively.

Figure 3b shows that type-II heterojunction with staggered band structure is fundamentally different from the type-I. The CB and VB levels of SC_A are both higher than those of SC_B. And the electrons and holes are not on the same semiconductor, and thus the e^- - h^+ recombination rate on the same semiconductor is effectively inhibited.

P-n heterojunction is proposed based on type-II heterojunctions (Figure 3c). Due to the presence of internal electric field (IEF), photogenerated electrons and holes are concentrated in the p- and n-regions, respectively. Consequently, electrons and holes are spatially separated and thus improve photocatalysis. Compared with type-I heterojunction, p-n/type-II heterojunctions can greatly enhance the charge carrier separation in space owing to the existence of IEF.[23]

Unlike the classical heterojunctions (*i.e.*, type-I/II, and p-n heterojunctions), the photogenerated electrons and holes of Z- and S-scheme heterojunction (Figure 3d) are accumulated at high oxidation and reduction potentials (OP and RP) and thus minimize the charge recombination, which can efficiently achieve the separation of e^- - h^+ pairs with simultaneously maximized reduction and oxidation capacities.[21,22]

Typically, the Z-scheme heterojunctions consist of two staggered semiconductors and a redox electron mediator pair,

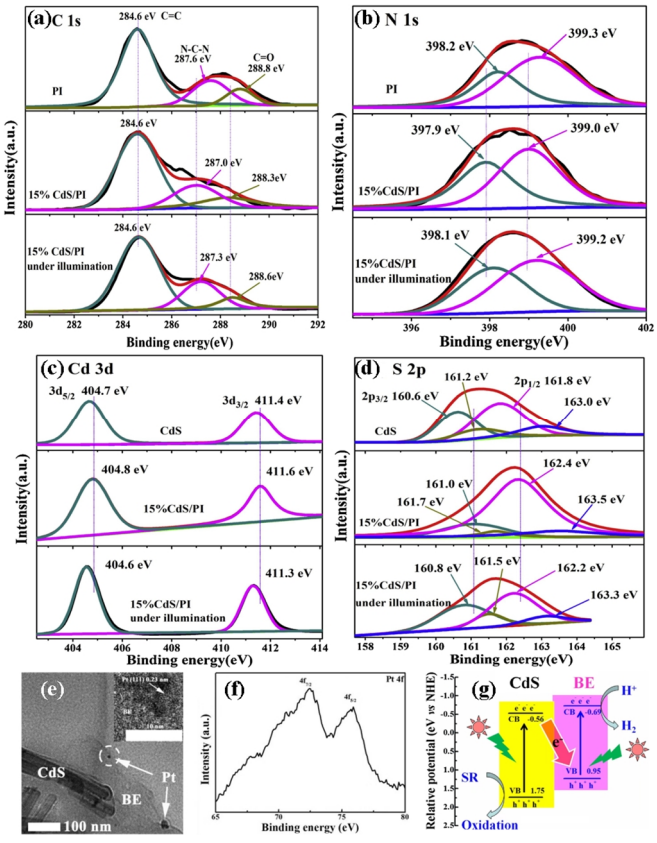

Figure 4. *Ex-situ* and *in-situ* XPS spectra of (a) C *1s*, (b) N *1s* of PI and 15% CdS/PI, (c) Cd *3d* and (d) S *2p* of CdS and 15% CdS/PI.[24] (e) TEM, HRTEM images, (f) Pt XPS spectrum of BE-CdS-10.0 hybrid after *in-situ* photodeposition of Pt from H_2PtCl_6, (g) Proposed photocatalytic H_2 production mechanism.[20]

wherein a larger potential offset is needed to make electron acceptors and donators to accept and donate electrons, respectively, which may lead to the weakened reduction and oxidation capacity. On the other hand, the S-scheme heterojunction consists of both reduction and oxidation photocatalysts, wherein the three major factors including the band bending, built-in electric field, and Coulomb force have been well combined, which retains the highest reduction and oxidation capacities of two semiconductors. Because of this advantage, S-scheme heterojunctions have been intensively studied in recent years.

Characterizations of Heterojunctions. The characterization methods for varied heterojunctions include *in-situ* XPS, noble metal deposition, radical capture experiments and theoretical calculations. For p-n heterojunction, the Mott-Schottky (M-S) typically shows "V" or inverted "V" shape characters owing to the presence of internal electric field.[18] The verification methods of S-scheme heterojunction have been summarized by Yu et al.[21] Direct Z-scheme heterojunction represents one of the most efficient photocatalytic protocols.[24,25]

***In-situ* XPS.** The variation of binding energy can directly reflect the changes of surface electron density, and the decrease of electron density leads to the increase of binding energy. Therefore, the direction of charge can be detected by the change of binding energy. *In-situ* XPS measurement can detect migration direction of electrons by measuring changes in the binding energy of elements under light irradiation compared with those measured in darkness. Wang et al. reported ultrathin nanosheets polyimide (PI) formed polymer-inorganic hybrid with CdS, in which 15% CdS/PI showed the highest performance due to the direct Z-scheme formation.[24] As the XPS spectra shown in Figure 4a and b, the C *1s* and N *1s* signals shift to higher binding energy for CdS/PI under light irradiation compared to those tested in darkness. On contrary, the binding energies of Cd *3d* and S *2p* under visible-light irradiation decreased (Figures 4c-d). These *in-situ* XPS analyses reveal that the photoinduced electrons in PI can migrate to CdS under light irradiation, suggesting the formation of direct Z-scheme CdS/PI heterojunction.

Noble Metal Deposition. Noble metals can be selectively deposited on the electron-rich region, which can reveal the region holding photogenerated electrons, thus confirming the charge carrier transfer route. Chen group reported organic/inorganic hybrid (BE/CdS) prepared from modified conjugated polybenzothiazole (B-BT-1,4-E, noted as BE) flake and CdS nanorods.[20] In the presence of a semiconductor, Pt^{4+} in H_2PtCl_6 was reduced to Pt^0 under light irradiation. TEM and corresponding HRTEM images of BE/CdS hybrids (Figure 4e) confirmed that Pt nanoparticles were loaded on BE rather than CdS. The XPS spectra of Pt showed that the binding energies of Pt $4f_{7/2}$ and $4f_{5/2}$ are 72.3 and 75.5 eV (Figure 4f), respectively, which nearly equal to the standard energy of zero Pt, implying the presence of Pt^0, and the electron is migrated from CB of CdS to the VB of BE *via* a Z-scheme instead of type II mechanism (Figure 4g).

Radical Capture Experiments. $^{\bullet}OH^-$ and $^{\bullet}O_2^-$ are two commonly used radicals for detection experiments, which can be captured by benzoquinone (BQ) and isopropylalcohol (IPA), respec-

DOI: 10.14102/j.cnki.0254-5861.2022-0188

Table 1. Summarized Preparation Methods of P-I Heterojunction Photocatalysts

Catalysts	Dosage (mg)	Preparation method	Ref.
BE-CdS	30	*in-situ* polycondensation	[20]
DBTSO@TiO_2	10	*in-situ* polycondensation	[26]
PyOT@TiO_2	10	*in-situ* polymerization	[27]
BBT/TiO_2	10	*in-situ* polymerization	[28]
BE-Au-TiO_2	30	*in-situ* polymerization	[29]
DPP-Car/TiO_2	100	*in-situ* polymerization	[30]
WO_3@TiO_2	20	*in-situ* chemical deposition method	[31]
CdS/PI	50	solvothermal method	[24]
g-C_3N_4/$BiVO_4$	80	hydrothermal method	[32]
Fe_2O_3/g-C_3N_4	50	electrostatic self-assembly approach	[33]
g-C_3N_4@BiOI	50	electrostatic self-assembly approach	[34]
Ag_3PO_4/PDI	20	self-assembly approach	[35]
g-C_3N_4/$Bi_4Ti_3O_{12}$	-	ball milling	[36]
g-C_3N_4/Bi_4NbO_8Cl	100	ball milling	[37]
BE/black TiO_2	30	ball milling	[38]
g-C_3N_4/MnO_2	-	wet-chemical method	[39]
CP/g-C_3N_4	50	molecular engineering strategy	[40]
P3HT/g-C_3N_4	10	facile rotary evaporation	[41]
CdS-DETA	50	microwave hydrothermal method	[42]
PPy/TiO_2	50	reverse microemulsion polymerization	[43]
(PANI)/TiO_2	-	hydrothermal-chemisorption process	[44]
ZnONRs-PANI	-	electrophoretic deposition	[45]
WO_3@Cu@PDI	5	water bath method	[46]
(TNZnPc)/TiO_2	-	electrospinning and solvothermal method	[47]

tively. For instance, g-C_3N_4-AQ-MoO_3 hybrid photocatalyst exhibits its excellent photocatalytic performance by the formation of Z-scheme heterojunction.[25] The $^{\bullet}OH$ and $^{\bullet}O_2^-$ radical signals in g-C_3N_4, MoO_3, and g-C_3N_4-AQ-MoO_3 were studied by DMPO spin-trapping ESR spectra. Under light irradiation, g-C_3N_4-AQ-MoO_3 hybrid possesses both DMPO-$^{\bullet}O_2^-$ and DMPO-$^{\bullet}OH$ signals, demonstrating the formation of Z-scheme heterojunction.

n PREPARATION METHODS OF P-I PHOTOCATALYTIC HETEROSTRUCTURES

The preparation methods of P-I heterojunction photocatalysts mainly include in situ polymerization, hydrothermal and solvothermal treatment, electrostatic self-assembly, ball milling methods, *etc*. Table 1 summarizes the preparation methods of P-I heterojunction photocatalysts.

***In-situ* Polymerization.** In situ polymerization, featured by simplicity and tightly bound interface, represents one of the most widely used methods for the synthesis of heterostructures.[26-31] Our previous work reported PyOT@TiO_2 polymer-inorganic heterojunctions can be smoothly constructed by an *in-situ* direct C-H arylation polycondensation.[27] Meanwhile, the mechanically

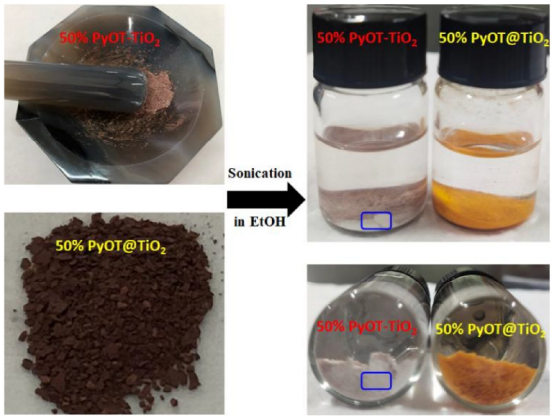

Figure 5. Mechanically mixed 50% PyOT-TiO_2 and *in situ* prepared 50% PyOT@TiO_2, and the images of their ultrasonic dispersions in EtOH.[27]

mixed 50% PyOT-TiO_2 was also prepared to make comparable study with the *in-situ* synthesized 50% PyOT@TiO_2. After being sonicated in ethanol and standing for a few mins (Figure 5), two separated phases, *i.e.*, reddish-brown PyOT and white TiO_2, can be distinctly observed in 50% PyOT-TiO_2. In sharp contrast to the mechanically mixed 50% PyOT-TiO_2, a stable and uniformed single phase still retains for the *in-situ* prepared 50% PyOT @TiO_2, showing that PyOT has been tightly bonded on the surface of TiO_2 particles, and there must be a strong interaction between PyOT and TiO_2.

Hydrothermal and Solvothermal Methods. Typically, a hydrothermal process is carried out under high pressure as well as temperature in autoclaves, resulting in high crystallinity and narrow particle size distribution of the synthesized semiconductor nanoparticles.[24,32] The solvothermal synthesis process is similar to the hydrothermal synthesis except for using different solvents. Organic solvents are commonly utilized in solvothermal process.

Electrostatic Self-assembly Method. The electrostatic self-assembly method is based on the electrostatic interaction of polyelectrolyte with opposite charge. Electrostatic self-assembly does not need to form chemical bonds, which can be easily operated and has high stability.[33-35]

Ball Milling. Ball milling is a facile, efficient and green technology for the synthesis of composite photocatalysts with minimal or no involvement of solvent.[36-38] Besides the abovementioned methods, other methods including wet chemical method,[39] molecular engineering strategy,[40] facile rotary evaporation,[41] microwave hydrothermal method,[42] reverse microemulsion polymerization,[43] hydrothermal-chemisorption process,[44] electrophoretic deposition,[45] water bath method,[46] electrospinning technique and solvothermal processing[47] have also been developed for the preparation of P-I heterostructures.

n PHOTOCATALYTIC APPLICATIONS OF P-I HETEROSTRUCTURES

Polymer-inorganic heterostructures have been widely used in photocatalytic hydrogen or oxygen evolution, CO_2 reduction and environmental remediation.[48,49]

Chin. J. Struct. Chem. **2022**, 41, 2209056-2209068
DOI: 10.14102/j.cnki.0254-5861.2022-0188

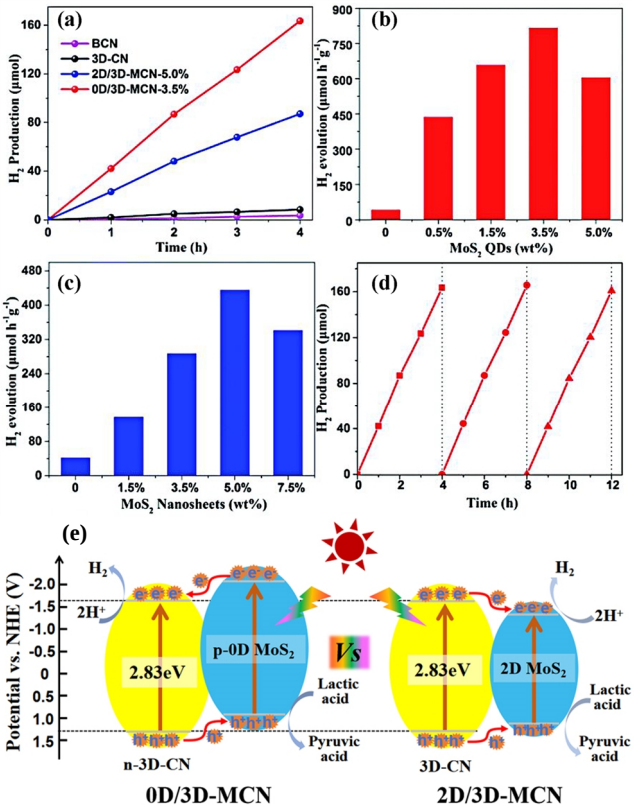

Figure 6. (a) The rate curves of samples for photocatalytic H_2 production, (b) the effect of the 0D-MoS_2 QDs amount, (c) HER of 2D-MoS_2 nanosheets, (d) recircling test of 0D/3D-MCN-3.5%, (e) proposed photocatalytic mechanisms for the 0D/3D-MCN and 2D/3D-MCN composites.[18]

Photocatalytic Water Splitting. Photocatalytic hydrogen production from water splitting has been regarded as one of the most important technologies for converting renewable solar energy to clean fuels. The main obstacle of photocatalytic overall water splitting is the half-reaction of oxygen generation that involves a four-electron pathway with a slow kinetics. Thereby, in many cases, sacrificial agents are required to consume holes or electrons, which correspond to sacrificial electron donors (SED) and sacrificial electron acceptors (SEA), respectively. SED, including lactic acid (LA), ascorbic acid (AA), triethanolamine (TEOA), triethanolamine (TEA), Na_2S, Na_2SO_3, methanol (MeOH) and ethanol (EtOH), are consumable to valence band holes, while SEA agents, such as $AgNO_3$ and ferric chloride ($FeCl_3$), consume conduction band electrons.

Similar to the most widely studied inorganic TiO_2-based photocatalysts, g-C_3N_4-based polymeric photocatalysts have also received extensive attention owing to its tunable synthetic methods, high specific surface area, low cost, high stability, and unique optical and electronic properties. Meanwhile, various inorganic photocatalysts have been integrated with g-C_3N_4 to build P-I heterojunctions.[18,23,50] Zhu *et al*. reported the transformation of MoS_2 morphology from 0D to 2D and 3D porous structures coupling with 2D-g-C_3N_4 to synthesize 0D (2D, 3D)-MoS_2/g-C_3N_4 photocatalysts for PHP application (Figure 6a-d).[18] 0D-MoS_2 quantum dots and 2D-MoS_2 nanosheets were first introduced onto 3D-CN to construct 0D/3D-MCN and 2D/3D-MCN through facile impregnation and *in situ* photo-deposition method. The effect of the MoS_2-covered 2D gC_3N_4 morphologies on PHP was systematically investigated. Changing the morphology of g-C_3N_4 from 2D to 3D porous structure is beneficial to gain more surface-active sites, higher transfer efficiency and larger specific surface area. This work highlights that modulating the morphology of MoS_2 can affect the charge transfer pathway of 0D/3D-MCN and 2D/3D-MCN heterostructures (Figure 6e).

Besides g-C_3N_4, other π-conjugated polymers (CP) and inorganic semiconductors heterojunctions for photocatalytic H_2 production have also been developed.[26,27,51-56] P-I heterojunction photocatalysts rationally combine respective advantages of polymer and inorganic semiconductors to improve the photocatalytic performance. Most of heterojunctions between the conjugated polymer materials and inorganic semiconductor are prepared by an *in-situ* synthetic strategy. Wang group reported poly(dibenzothiophene-S,S-dioxide)@TiO_2 nanoparticles (PDBT- SO@TiO_2) composite through *in situ* polymerization, which exhibit the highest HER up to 51.5 mmol $h^{-1}g^{-1}$.[26]

Yu group developed an S-scheme heterojunction photocatalyst between a pyrene-based CP, *i.e.*, pyrene-alt-triphenylamine (PT) and CdS nanocrystals (Figure 7a-e). The optimal CdS/PT hybrid,

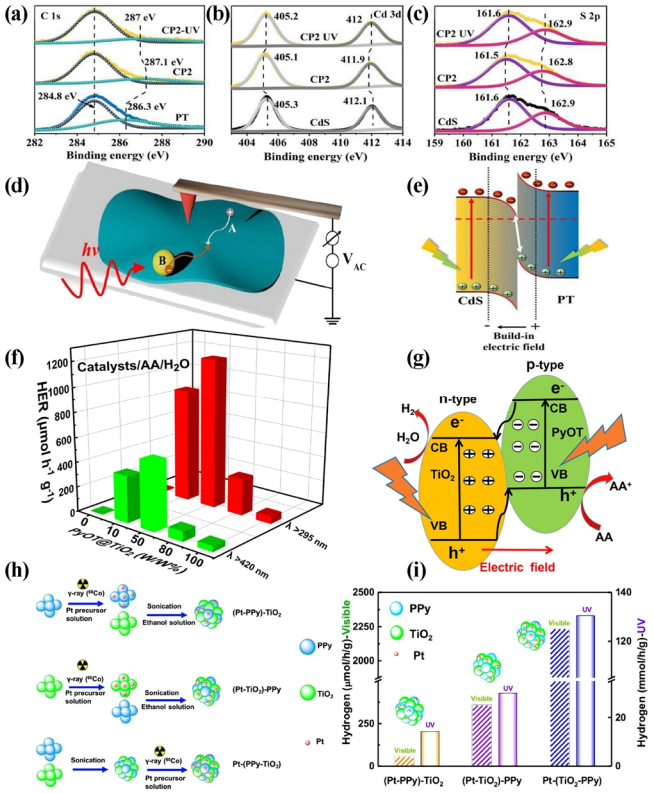

Figure 7. (a-c) High-resolution XPS spectra, (d) schematic illustration of photoirradiation KPFM, (e) schematic illustration of S-scheme charge transfer process.[51] (f) Normalized HERs under visible or full arc light, (g) p-n heterojunction of PyOT@TiO_2.[27] (h) Schematic diagram of catalysts synthesis, (i) hydrogen production by (Pt-PPy)-TiO_2, (Pt-TiO_2)-PPy and Pt-(PPy-TiO_2).[52]

DOI: 10.14102/j.cnki.0254-5861.2022-0188

integrating 2 wt% PT with CdS and 1 wt% Pt as cocatalyst, exhibited an outstanding HER of 9.28 mmol $h^{-1}g^{-1}$ with an apparent quantum efficiency (AQE) up to 24.3%, which is about 8 times higher than that of pristine CdS. Kelvin probe force microscopy (KPFM) and *in-situ* XPS analyses fully demonstrate the mechanism of S-scheme charge transfer.[51] Importantly, the C 1s peaks of CP2, and the Cd 3d and S 2p peaks of CdS negatively and positively shifted under light irradiation, respectively, as compared to those in dark, proving the photoelectron transfer direction from CdS to PT.

Our group reported the P-I (PyOT@TiO_2) heterojunctions that are built *via in-situ* C-H arylation polycondensation. All resultant heterostructures, including 10%, 50% and 80% PyOT @TiO_2, exhibited much higher HERs compared to the pristine TiO_2 and PyOT either under visible or full-arc irradiation. 50% PyOT@TiO_2 dispersed in an ascorbic acid (AA) aqueous solution (pH = 4) shows the highest HER in the absence of Pt co-catalyst (Figure 7f). P-n heterojunction charge transfer that contributes to the enhanced photocatalytic performance was revealed by M-S plot and •OH detection experiments.[27]

Remita et al. designed a P-I heterostructure (Figure 7h-i) based on ternary polypyrrole PPy-TiO_2 nanocomposites with 2 nm-Pt nanoparticles, *i.e.*, (Pt-PPy)-TiO_2, (Pt-TiO_2)-PPy and Pt-(PPy-TiO_2). Photocatalytic hydrogen evolution tests in 25% MeOH aqueous solution reveal that Pt-(PPy-TiO_2) nanostructures with co-deposition of Pt nanoparticles on TiO_2 and PPy show much higher HER than(Pt-PPy)-TiO_2 and (Pt-TiO_2)-PPy irradiated either by UV or visible light.[52]

Zhang et al. designed reduced graphite oxide/CdS-DETA (PRGO/CdS-DETA) porous composites with excellent PHP performance and stability.[53] Chen group synthesized CMPs with different structures by Sonogashira coupling polycondensation between 4,7-dibromobenzo[c][1,2,5]thiadiazole and 1,3,5-triethynylbenzene to construct heterojunctions with inorganic semiconductors TiO_2 and CdS for both PHP and photocatalytic degradation applications.[20,28,54] Multifunctional π-conjugated microporous poly(benzothiadiazole)/TiO_2 (BBT/TiO_2) heterojunction through an *in-situ* polycondensation can dramatically improve the photocatalytic activity for H_2 evolution and degradation of ciprofloxacin under the visible light.[28] The possible mechanisms of PHP and CIP photodegradation for BBT/TiO_2 heterojunction are proposed as shown in Figure 8 (a-b). To further improve the photocatalytic performance of conjugated polymer-TiO_2 composites, a linear conjugated polymer (benzothiadiazole) (B-BT-1, 4-E) was employed to form a binary composite heterojunction with TiO_2 *via* a facile *in-situ* strategy (Figure 8 c).[54] As a result, B-BT-1,4-E/TiO_2 showed a wider visible light absorption and more efficient charge mobility than CMP-based BBT/TiO_2. Besides, a new type of polymer/inorganic hybrid using modified conjugated polybenzothiadiazole (B-BT-1,4-E, noted as BE) flake and CdS nanorod was also developed by the same group.[20] Based on the comprehensive photocatalytic experiments, the HER of optimal BE-CdS hybrid was 8.3 and 23.3 times higher than those of CdS and BE, respectively, attributing to broader visible/near-infrared (vis/NIR) light absorption region (400-700 nm) and rapid photogenerated e^-/h^+ separation owing to the formation of Z-scheme heterojunction.[20]

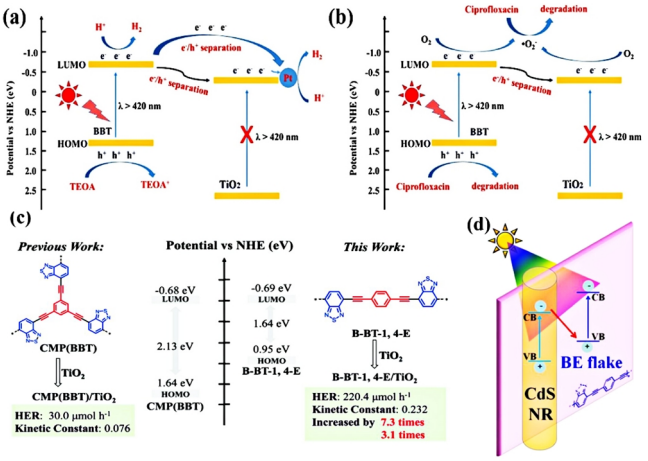

Figure 8. Proposed mechanism for (a) photocatalytic H_2 production, (b) photodegradation of CIP over BBT-TiO_2 heterojunction.[28] (c) *In situ* fabrication of B-BT-1,4-E on the surface of TiO_2.[54] (d) Configuration of energy band positions and Z-scheme photogenerated charge carrier transfer in the BE-CdS hybrid photocatalyst.[20]

Yan et al. reported photocatalytic oxygen evolution by Fe_2O_3/C_3N_4 and Fe_2O_3/C-C_3N_4 heterojunctions, respectively, which were about 10- and 30-folds higher than that of pristine g-C_3N_4, showing the presence of strong interaction between amorphous carbon and Fe_2O_3.[56] In addition, oxygen evolution at λ = 450, 470 and 500 nm was also studied, demonstrating that heterostructures can boost the electron and hole pairs migration, separation, and thus photocatalytic reaction.

Zhang et al. reported polymer/inorganic g-C_3N_4/CoN nitride heterostructure realizes more than 4-fold enhancement in catalytic activity for O_2 evolution compared to the bare g-C_3N_4, with a highest O_2 evolution rate up to 607.2 μmol $g^{-1}h^{-1}$ under visible light.[57] Cooper et al. reported a Z-scheme photocatalyst consisting of linearly conjugated polymers and $BiVO_4$ used for overall water splitting under visible light.[58] Zhao et al. reported a C_3N_4 and WO_3-based heterostructure photocatalyst *via* a facile hydrothermal strategy for mediator-free overall water splitting. And the excellent C_3N_4-WO_3 composite has the highest H_2/O_2 production rate (2.84 and 1.46 μmol h^{-1}, respectively) and the quantum yield is 0.9%.[59]

Photocatalytic overall water splitting without sacrificial agents represents one of the most ideal protocols for solar to chemical energy conversions. Although overall water splitting seems very fascinating, it is a thermodynamically up-hill process (ΔG_0 = 237.13 kJ·mol^{-1}), which is still far from the practical applications owing to the low solar-to-hydrogen (STH) conversion efficiency. Wang et al. designed Fe_2O_3/reduced graphene oxide/polymer carbon nitride (Fe_2O_3/RGO/PCN) ternary heterojunction (RGO nanosheets as solid mediators) to accelerate carrier transfer and achieve an efficient photocatalytic performance for the overall water splitting.[60] The photocatalytic H_2 and O_2 production rates of PCN in the presence of Pt were, respectively, 20.9 and 9.4 μmol h^{-1}, with a 2:1 stoichiometric ratio for H_2:O_2. When Fe_2O_3 nanoparticles were added into PCN, the water splitting activity was slightly higher than that of pure PCN. Impressively, when RGO

DOI: 10.14102/j.cnki.0254-5861.2022-0188

nanosheets were used as a solid electronic medium to connect the hydrogen and oxygen evolution photocatalysts, the optimum overall water splitting activity could be further enhanced (H_2: 43.6 μmol h^{-1} and O_2: 21.2 μmol h^{-1}). Table 2. summarizes the photocatalytic water splitting of reported P-I heterostructures.

CO_2 Reduction. Inspired by natural photosynthesis, photocatalytic conversion of CO_2 into other carbon-containing products such as hydrocarbon or alcohol chemical fuels has attracted extensive attention.[61-66] In 1979, Inoue *et al.* reported, for the first time, the reduction of CO_2 to CO, CH_4, CH_3OH, HCOOH and other carbon-based fuels using semiconductor photoelectricity catalysis. Nevertheless, photocatalytic CO_2 reduction is a multiple-step reaction with a large uphill thermodynamic barrier, which is still an ongoing and challenging topic.

Ding group developed an α-Fe_2O_3/g-C_3N_4 (FCN) hybrid for photocatalytic CO_2 reduction (Figure 9a).[67] The total photocatalytic CH_3OH evolution rates of α-Fe_2O_3, g-C_3N_4 and FCN hybrid were compared. There is no CH_3OH product for pristine α-Fe_2O_3, and photocatalytic activity of the pure g-C_3N_4 for CO_2 reduction is only 1.94 μmol $h^{-1}g^{-1}$. For FCN hybrids, the effect of the varied mass ratio of α-Fe_2O_3 to g-C_3N_4 on CH_3OH production was investigated. As a result, the FCN hybrid with a 40:60 ratio exhibited the highest CH_3OH production rate (5.63 μmol $h^{-1}g^{-1}$), which is approximately 2.9 times higher than that of single-component g-C_3N_4. Mechanism study showed that the PL intensity of FCN (40:60) is much lower than that of pure g-C_3N_4 (Figure 9b), indicating the presence of Fe element can effectively reduce the recombination of photogenerated electron-hole pairs. Wong group reported a hierarchical direct Z-scheme system combining 3D urchin-like α-Fe_2O_3 and g-C_3N_4 photocatalysts. It provides an enhanced photocatalytic activity of reduction of CO_2 to CO, yielding a CO evolution rate of 27.2 μmol $h^{-1}g^{-1}$ in the absence of cocatalyst as well as sacrifice agent (Figure 9c),[68] which is about 2.2 times higher than

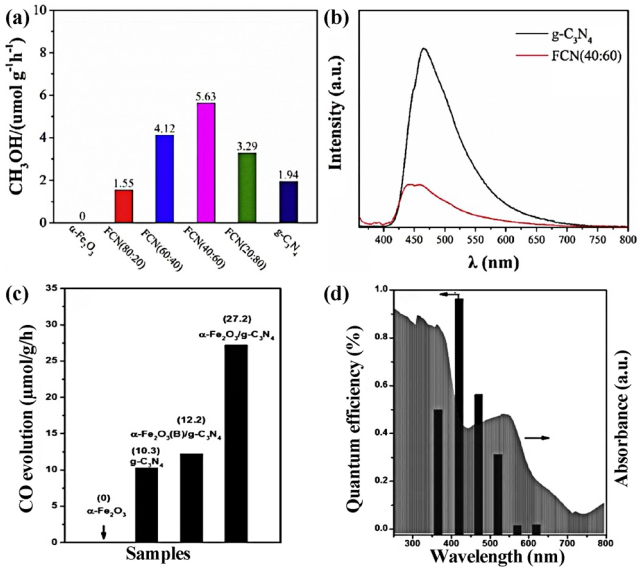

Figure 9. (a) Average CH_3OH production rates of g-C_3N_4, α-Fe_2O_3 and FCN hybrid, (b) PL spectra of CN and FCN (40:60).[67] (c) Average CO production rates of g-C_3N_4, α-Fe_2O_3, and α-Fe_2O_3/g-C_3N_4 hybrid, (d) wavelength dependence of QE of α-Fe_2O_3/g-C_3N_4.[68]

Table 2. Summary of Reported P-I Heterostructures for Photocatalytic Water Splitting

Catalysts	Cocatalyst	Sacrificial reagent	Activity (μmol $h^{-1}g^{-1}$)	AQE (420 nm)	Ref.
MoS_2/g-C_3N_4	-	lactic acid	H_2: 817.1	-	[18]
BE-CdS	1.0 wt% Pt	Na_2S/Na_2SO_3	H_2: 40990	7.5%	[20]
CoOx@g-C_3N_4	-	TEA	H_2: 262.9	1.9%	[23]
PDBTSO@TiO_2	3.0 wt% Pt	TEOA	H_2: 51500	13%	[26]
PyOT@TiO_2	-	AA	H_2: 1200	-	[27]
BBT/TiO_2	0.3 wt% Pt,	TEOA	H_2: 6750	1.45% (450 nm)	[28]
BE-Au-TiO_2	1.0 wt% Pt	TEOA	H_2: 26040	7.8%	[29]
CdS/PI	1.0 wt% Pt	lactic acid	H_2: 613	-	[24]
Fe_2O_3/g-C_3N_4	1.0 wt % Pt	TEOA	H_2: 398.0	-	[33]
TiO_2/C_3N_4	1.0 wt %Pt	TEOA	H_2: 1540	4.94% (365 nm)	[50]
CdS/PT	1 wt% Pt	lactic acid	H_2: 9280	24.3% (400 nm)	[51]
PPy-TiO_2	1 wt% Pt	CH_3OH	H_2: 3200	-	[52]
PRGO/CdS-DETA	0.6 wt% Pt	Na_2S/Na_2SO_3	H_2: 10500	29.5%	[53]
B-BT-1,4-E/TiO_2	-	TEOA	H_2: 7346.7	1.91%	[54]
g-C_3N_4/$CdCO_3$/CdS	3 wt% Pt	Na_2S/Na_2SO_3	H_2: 3521	-	[55]
g-C_3N_4-AQ-MoO_3	2 wt% Pt	TEOA	H_2: 2999	-	[25]
Fe_2O_3/C-C_3N_4	-	$AgNO_3$	O_2: 223	-	[56]
g-C_3N_4/CoN	-	$AgNO_3$	O_2: 607.2	-	[57]
P10/$BiVO_4$	-	-	H_2: 5.0	-	[58]
			O_2: 2.7		
C_3N_4-rGO-WO_3	1.0 wt % Pt	-	H_2: 12.4	0.9%	[59]
			O_2: 7.3		
Fe_2O_3/RGO/PCN	-	-	H_2: 1090	-	[60]
			O_2: 530		

DOI: 10.14102/j.cnki.0254-5861.2022-0188

Table 3. Reaction Conditions and Photocatalytic Activities of P-I Heterojunctions for CO_2 Reduction

Catalysts	Mass (mg)	Products evolution rate (μmol $h^{-1}g^{-1}$)	AQY (%)	Ref.
α-Fe_2O_3/g-C_3N_4	10	CH_3OH (5.63)	-	[67]
α-Fe_2O_3/g-C_3N_4	25	CO (27.2)	0.499 (365 nm)	[68]
Co-MOF/Cu_2O	20	CO (3.83)	-	[70]
g-C_3N_4/SnS_2	50	CH_4 (0.21) CH_3OH (0.77)	-	[71]
g-C_3N_4/WO_3	3	CH_3OH (1.1)	-	[72]
g-C_3N_4/ZnO	100	CH_3OH (0.6)	-	[73]
AgCl@g-C_3N_4	300	CH_4 (25.67) CH_3COOH (1.2) HCOOH (0.67)	0.211 (475 nm)	[74]
$NiTiO_3$/g-C_3N_4	10	CH_3OH (13.74)	-	[75]
Au@g-C_3N_4/SnS	50	CH_4 (3.8) CH_3OH (5.3)	15.3 (525 nm)	[76]
BN@Zn/Co-ZIF	20	CO (152.2)	-	[77]
CPDs/$Bi_4O_5Br_2$	30	CO (132.42)	0.81 (380 nm)	[78]
SnO_{2-x}/g-C_3N_4	20	CH_3OH (3)	-	[79]
$FeTiO_3$/TiO_2	50	CH_3OH (0.462)	-	[80]
Ag_3PO_4/g-C_3N_4	10	CO (44) CH_3OH (9) CH_4 (0.2) C_2H_5OH (0.1)	-	[81]
CeO_2/g-C_3N_4	50	CO (11.8) CH_4 (9.08)	-	[82]

that of the pristine g-C_3N_4 (10.3 μmol $h^{-1}g^{-1}$). The wavelength dependence of quantum efficiency (QE) for α-Fe_2O_3/g-C_3N_4 hybrid achieved 0.499% and 0.963% at λ = 365 and 420 nm, respectively (Figure 9d). Wang group designed inorganic-organic hybrid photocatalysts to enhance the reduction of CO_2 under visible light. A Mn complex was installed onto Bi_2WO_6 *via* bisphosphonate groups, which possess advantages of low cost and high efficiency toward CO_2 reduction.[69] Li group reported a Co-MOF/Cu_2O heterojunction with high selectivity for the visible light-driven reduction of CO_2 to CO without using any photosensitizer and sacrificial reagents. This p-n heterojunction Co-MOF/Cu_2O hybrid composite (xCMC) exhibited remarkable CO production rate of 3.83 μmol $g^{-1}h^{-1}$, which is 9.6-fold higher than that of single-component Cu_2O.[70]

Besides the abovementioned examples, many other P-I heterojunction photocatalysts for CO_2 reduction, such as g-C_3N_4/ SnS_2,[71] g-C_3N_4/WO_3,[72] g-C_3N_4/ZnO,[73] AgCl@g-C_3N_4,[74] $NiTiO_3$/ g-C_3N_4,[75] Au@g-C_3N_4/SnS,[76] and p-BN@Zn/Co-ZIF,[77] carbonized polymer dots/$Bi_4O_5Br_2$,[78] SnO_{2-x}/g-C_3N_4,[79] $FeTiO_3$/TiO_2,[80] Ag_3PO_4/g-C_3N_4,[81] and CeO_2/g-C_3N_4[82] have also been developed, all of which show enhanced photocatalytic activities compared to the single-component photocatalysts. Table 3 summarizes the recent reports on the P-I heterostructures for photocatalytic CO_2 Reduction.

Environmental Remediation. Water pollution is mainly faced with extremely complex components with the characteristics of high concentration, difficult degradation and lasting toxicity, representing one of the most serious threats to human life. Phenols, polycyclic aromatic hydrocarbons, ammonia nitrogen, cyanide, sulfide and other harmful substances are the main sources of organic pollutants. Copious strategies to environmental remediation, including physical adsorption, chemical degradation, biodegradation, and photocatalytic degradation, have been developed.[83-86] Among which, semiconductor-mediated photocatalytic pollutant degradation, as a green and promising method, has attracted extensive attention.

Yu group reported a direct Z-scheme photocatalyst based on 2D/2D g-C_3N_4/MnO_2 nanocomposite for dye degradation and phenol removal with enhanced activity (Figure 10a-b).[39] The degradation rate of RhB by g-C_3N_4/MnO_2 composites achieved as high as 91.3% after irradiation for 60 min, while those of g-C_3N_4 and MnO_2 were only 19.6% and 22.3%, respectively. Based on the Langmuir-Hinshelwood model, their decomposition behavior is consistent with the pseudo-first-order kinetics and the apparent rate constant of the g-C_3N_4/MnO_2 nanocomposite was 0.033 min, about ~9 and ~5 times higher than those of pristine g-C_3N_4 and

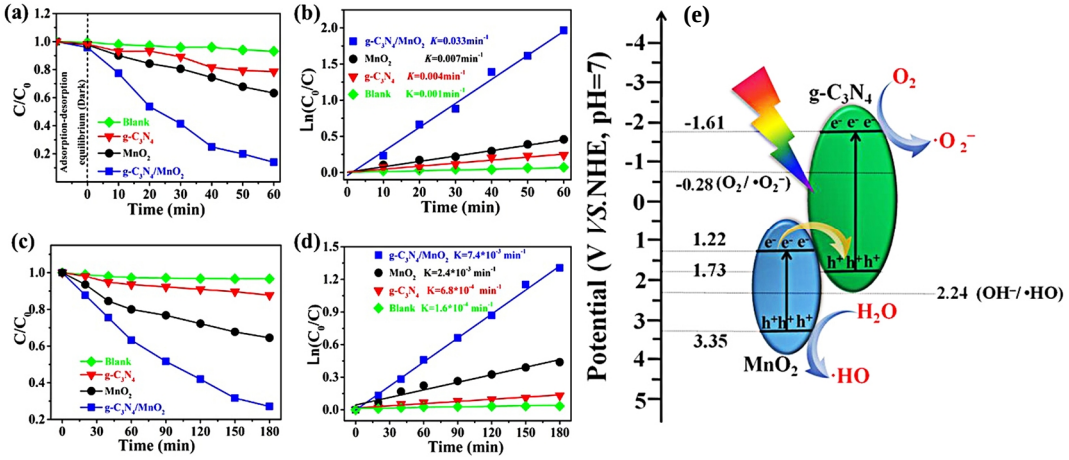

Figure 10. Photocatalytic degradation rate of (a) RhB and (c) phenol. The kinetics fitted curves and apparent reaction rates of (b) RhB and (d) phenol, (e) mechanism of the g-C_3N_4/MnO_2 nanocomposite.[39]

Chin. J. Struct. Chem. **2022**, 41, 2209056-2209068
DOI: 10.14102/j.cnki.0254-5861.2022-0188

MnO_2, respectively. Moreover, the 2D/2D g-C_3N_4/MnO_2 also exhibit dramatically enhanced activity toward phenol removal (Figure 10c-d). Finally, the improved photocatalytic activity of g-C_3N_4/MnO_2 is mainly ascribed to the formation of Z-scheme heterojunction, as proved by Mott-Schottky measurement, electron paramagnetic resonance (EPR) and XPS spectra (Figure 10e).

Besides aforementioned cases, many other P-I heterojunction photocatalysts, such as CN/rGO@BPQDs,[87] CoO/g-C_3N_4,[88] α-Fe_2O_3/g-C_3N_4,[89] PPy/TiO_2,[43] Nb_2O_5/g-C_3N_4,[90] WO_3@Cu@PDI,[46] PDI/BiOCl,[91] g-C_3N_4/Cu_2O@Cu,[92] AgBr/P-g-C_3N_4,[93] and DPP-Car/TiO_2[30] have also been reported for organic pollutants degradation, showing enhanced photocatalytic activities for the degradation of various pollutants. Table 4 summarizes the recent reports on the P-I heterostructures for environmental remediation.

n CONCLUSIONS AND OUTLOOK

In this minireview, the synthesis, classification and applications of P-I heterojunctions are summarized and discussed. The mechanism and charge transfer pathway of P-I heterojunctions can be revealed by hydroxyl radical measurement, photocurrent measurements, *in-situ* XPS, M-S plot, DFT calculation, and so forth. Compared to single-component semiconductor photocatalysts, P-I heterojunction can combine the advantages of respective components, *i.e.*, polymeric and inorganic semiconductors, to improve the photocatalytic performance. Although P-I heterojunction photocatalysis has made enormous progress in recent years, there are some key issues that still need to be addressed.

Firstly, the preparation methods of P-I heterojunctions are relatively monotonous. *In-situ* polymerization is a major method for the preparation of P-I heterojunction photocatalysts. In the future, more attention should be paid to the rational design of preparation methods. Secondly, photocatalytic hydrogen or oxygen production from water splitting generally requires the addition of a hole or electron sacrificial agent. When the sacrificial agent is exhausted, the photocatalytic efficiency will be greatly reduced. Hence it is imperative to add sacrificial agent regularly, which is not conformed to the atomic economy and environmental protection that we are pursuing now. But it is still a great challenge to design superior photocatalysts without adding sacrificial agents to achieve the effect of photocatalytic water splitting. Finally, the exact photocatalytic mechanisms of P-I heterojunctions still need to be further revealed. For example, the reaction mechanism of photocatalytic CO_2 reduction is still ambiguous, and the optimal reaction path and active intermediates are also controversial. And the study of heterojunction mechanism is still a great challenge.

Although some encouraging results have been achieved so far, the stability and efficiency of P-I hybrid nanocomposites are still far from satisfying the requirements of large-scale application. There is an urgent need to develop green, atom-economic,[26,95,96] efficient and multifunctional P-I heterojunctions with controllable morphology, defined structure, broad light harvesting, excellent charge carrier mobility, and well-matched energy level. The P-I heterojunctions based on electron donor-acceptor (D-A) types of polymers[97] are also expected to possess synergetic effect on the enhancement of charge separation. Considering that conjugated polymers typically have high-lying conduction band with strong reductive capacity, the heterojunctions based on the combination of π-conjugated polymer with a second inorganic semiconductor that have a deep-lying valence band are expected to achieve the separation of electron hole pairs with simultaneously maximized reduction and oxidation capacities, and thus provide great opportunity for photocatalytic overall water splitting.

Table 4. Reaction Conditions and Photocatalytic Activities of P-I Heterojunctions for Pollutant Degradation

Catalyst	Pollutant concentration (mg L^{-1})	Pollutants	Rate constant (k, min^{-1})	Ref.
MnO_2/g-C_3N_4	50	phenol	0.0407	[39]
CN/rGO@BPQDs	10	RhB[a]	0.183	[87]
	50	TC[b]	0.0194	
CoO/g-C_3N_4	10	TC[b]	0.0404	[88]
α-Fe_2O_3/g-C_3N_4	-	NO	0.0156	[89]
PPy/TiO_2	20	MO[c]	0.0089	[43]
Nb_2O_5/g-C_3N_4	20	TC[b]	0.0096	[90]
WO_3@Cu@PDI	20	TC[b]	0.08	[46]
PDI/BiOCl	5	phenol	0.013	[91]
g-C_3N_4/Cu_2O@Cu	15	BPS[c]	0.0062	[92]
AgBr/P-g-C_3N_4	0.1	EPH[d]	0.0409	[93]
$Bi_2Sn_2O_7$/PDIH	10	NOR[e]	0.4903	[94]
DPP-Car/TiO_2	10	MO[f]	0.0563	[30]

[a] Rhodamine B (RhB); [b] Tetracycline (TC); [c] Bisphenol-S (BPS); [d] Ephedrine (EPH); [e] Norfloxacin (NOR) and [f] Methyl ora (MO).

n ACKNOWLEDGEMENTS

The National Natural Science Foundation of China (Nos. 21374075 and 22169009), Jiangxi Provincial Natural Science Foundation (No. 20212ACB204007) and the Jiangxi Provincial Key Laboratory of Functional Molecular Materials Chemistry (20212BCD42018) are acknowledged for financial support.

n AUTHOR INFORMATION

Corresponding author. Email: chelsy@zju.edu.cn or chelsy@jxust.edu.cn (S.-Y. Liu)

n COMPETING INTERESTS

The authors declare no competing interests.

n ADDITIONAL INFORMATION

Full paper can be accessed via http://manu30.magtech.com.cn/jghx/EN/10.14102/j.cnki.0254-5861.2022-0188
For submission: https://www.editorialmanager.com/cjschem

n REFERENCES

(1) Wang, H.; Li, X.; Zhao, X.; Li, C.; Song, X.; Zhang, P.; Huo, P.; Li, X. A review on heterogeneous photocatalysis for environmental remediation: from semiconductors to modification strategies. *Chin. J. Catal.* **2022**, 43, 178-214.

(2) Wang, M.; Wu, X.; Wang, S.; Lu, C. A stable polyoxometalate-based coordination polymer for light driven degradation of organic dye pollutant. *Chin. J. Struct. Chem.* **2021**, 40, 1449-1455.

(3) Yuan, L.; Qi, M.; Tang, Z.; Xu, Y. Coupling strategy for CO_2 valoriza-

tion integrated with organic synthesis by heterogeneous photocatalysis. *Angew. Chem. Int. Ed.* **2021**, 60, 21150-21172.

(4) Su, T.; Shao, Q.; Qin, Z.; Guo, Z.; Wu, Z. Role of interfaces in two-dimensional photocatalyst for water splitting. *ACS Catal.* **2018**, 8, 2253-2276.

(5) Wu, H.; Miao, T.; Shi, H.; Xu, W.; Fu, X.; Qian, L. Probing photocatalytic hydrogen evolution of cobalt complexes: experimental and theoretical methods. *Chin. J. Struct. Chem.* **2021**, 40, 1696-1709.

(6) Fujishima, A.; Honda, K. Electrochemical photolysis of water at a semiconductor electrode. *Nature* **1972**, 238, 37-38.

(7) Yanagida, S.; Kabumoto, A.; Mizumoto, K.; Pac, C.; Yoshino, K. Poly(p-phenylene)-catalysed photoreduction of water to hydrogen. *J. Chem. Soc. Chem. Commun.* **1985**, 8, 474.

(8) Wang, X.; Maeda, K.; Thomas, A.; Takanabe, K.; Xin, G.; Carlsson, J.; Domen, K.; Antonietti, M. A metal-free polymeric photocatalyst for hydrogen production from water under visible light. *Nat. Mater.* **2009**, 8, 76-80.

(9) Lan, Z.; Ren, W.; Chen, X.; Zhang, Y.; Wang, X. Conjugated donor-acceptor polymer photocatalysts with electron-output “tentacles” for efficient hydrogen evolution. *Appl. Catal. B Environ.* **2019**, 245, 596.

(10) Cheng, J.-Z.; Liu, L.-L.; Liao, G.; Shen, Z.-Q.; Tan, Z.; Xing, Y.; Li, X.-X.; Yang, K.; Chen, L.; Liu, S.-Y. Achieving an unprecedented hydrogen evolution rate by solvent-exfoliated CPP-based photocatalysts. *J. Mater. Chem. A* **2020**, 8, 5890-5899.

(11) Lan, Z.; Zhang, G.; Chen, X.; Zhang, Y.; Zhang, K.; Wang, X. Reducing the exciton binding energy of donor-acceptor-based conjugated polymers to promote charge-induced reactions. *Angew. Chem. Int. Ed*. **2019**, 30, 10236-10240.

(12) Li, G.; Xie, Z.; Wang, Q.; Chen, X.; Zhang, Y.; Wang, X. Asymmetric acceptor-donor-acceptor polymers with fast charge carrier transfer for solar hydrogen production. *Chem. Eur. J.* **2021**, 27, 939-943.

(13) Li, G.; Wang, B.; Wang, R. g-C_3N_4/Ag/GO composite photocatalyst with efficient photocatalytic performance: synthesis, characterization, kinetic studies, toxicity assessment and degradation mechanism. *Chin. J. Struct. Chem.* **2020**, 39, 1675-1688.

(14) Low, J.; Yu, J.; Jaroniec, M.; Wageh, S.; Al-Ghamdi, A. Heterojunction photocatalysts. *Adv. Mater* **2017**, 29, 1601694.

(15) Li, H.; Li, X.; Lang, X. Extending the π-conjugated molecules on TiO_2 for the selective photocatalytic aerobic oxidation of suldes triggered by visible light. *Sustain. Energy Fuels* **2021**, 5, 2127-2135.

(16) Xu, F.; Zhang, L.; Cheng, B.; Yu, J. Direct Z-scheme TiO_2/NiS core-shell hybrid nanofibers with enhanced photocatalytic H_2-production activity. *ACS Sustain. Chem. Eng.* **2018**, 6, 12291-12298.

(17) Zhang, J.; Liao, H.; Sun, S. Construction of 1D/1D WO_3 nanorod/TiO_2 nanobelt hybrid heterostructure for photocatalytic application. *Chin. J. Struct. Chem.* **2020**, 39, 1019-1028.

(18) Zhou, B.; Yang, B.; Waqas, M.; Xiao, K.; Zhu, C.; Wu, L. Design of a p-n heterojunction in 0D/3D MoS_2/g-C_3N_4 composite for boosting the efficient separation of photogenerated carriers with enhanced visible-light-driven H_2 evolution. *RSC Adv.* **2020**, 10, 19169-19177.

(19) Zhao, B.; Zhao. Y.; Liu, P.; Men, Y.; Meng, X.; Pan, Y. Progress and understanding on catalysts with well-defined interface for boosting CO_2 conversion. *Chin. J. Struct. Chem.* **2022**, 41, 41324-41333.

(20) Zhang, X.; Xiao, J.; Hou, M.; Xiang, Y.; Chen, H. Robust visible/near-infrared light driven hydrogen generation over Z-scheme conjugated polymer/CdS hybrid. *Appl. Catal. B Environ.* **2018**, 224, 871-876.

(21) Xu, Q.; Zhang, L.; Cheng, B.; Fan, J.; Yu, J. S-Scheme heterojunction photocatalyst. *Chem* **2020**, 6, 1543-1559.

(22) Liao, G.; Li, C.; Liu, S.; Fang, B.; Yang, H. Emerging frontiers of Z-scheme photocatalytic systems. *Trends Chem.* **2022**, 4, 111-127.

(23) Zhu, Y.; Wan, T.; Wen, X.; Chu, D.; Jiang, Y. Tunable type I and II heterojunction of CoOx nanoparticles confined in g-C_3N_4 nanotubes for photocatalytic hydrogen production. *Appl. Catal. B Environ.* **2019**, 244, 814-822.

(24) Hu, Y.; Hao, X.; Cui, Z.; Zhou, J.; Chu, S.; Wang, Y.; Zou, Z. Enhanced photocarrier separation in conjugated polymer engineered CdS for direct Z-scheme photocatalytic hydrogen evolution. *Appl. Catal. B Environ.* **2020**, 260, 118131.

(25) Ma, X.; Wang, G.; Qin, L.; Liu, J.; Li, B.; Hu, Y.; Cheng, H. Z-scheme g-C_3N_4-AQ-MoO_3 photocatalyst with unique electron transfer channel and large reduction area for enhanced sunlight photocatalytic hydrogen production. *Appl. Catal. B Environ.* **2021**, 288, 120025.

(26) Shu, G.; Wang, Y.; Li, Y.; Zhang, S.; Jiang, J.; Wang, F. A high performance and low cost poly (dibenzothiophene-S, S-dioxide)@TiO_2 composite with hydrogen evolution rate up to 51.5 mmol h^{-1} g^{-1}. *J. Mater. Chem. A* **2020**, 8, 18292-18301.

(27) Xing, Y.-Q.; Tan, Z.; Cheng, J.; Shen, Z.; Zhang, Y.; Chen, L.; Liu, S.-Y. In situ C-H activation-derived polymer@TiO_2 p-n heterojunction for photocatalytic hydrogen evolution. *Sustain. Energy Fuels* **2021**, 5, 5166-5174.

(28) Hou, H.; Zhang, X.; Huang, D.; Ding, X.; Wang, S.; Yang, X.; Li, S.; Xiang, Y.; Chen, H. Conjugated microporous poly(benzothiadiazole)/TiO_2 heterojunction for visible-light-driven H_2 production and pollutant removal. *Appl. Catal. B Environ.* **2017**, 203, 563-571.

(29) Xiao, J.; Luo, Y.; Yang, Z.; Xiang, Y.; Zhang, X.; Chen, H. Synergistic design for enhancing solar-to-hydrogen conversion over TiO_2 based ternary hybrid. *Catal. Sci. Technol.* **2018**, 8, 2477-2487.

(30) Yang, L.; Yu, Y.; Zhang, J.; Chen, F.; Meng, X.; Qiu, Y.; Dan, Y.; Jiang, L. In-situ fabrication of diketopyrrolopyrrole-carbazole-based conjugated polymer/TiO_2 heterojunction for enhanced visible light photocatalysis. *Appl. Surf. Sci.* **2018**, 434, 796-805.

(31) Yang, X.; Fu, H.; Wang, W.; Xiong, S.; Han, D.; Deng, Z.; An, X. Enhanced solar light photocatalytic performance based on a novel Au-WO_3@TiO_2 ternary core-shell nanostructures. *Appl. Surf. Sci.* **2020**, 505, 144631.

(32) Lu, M.; Li, Q.; Zhang, C.; Fan, X.; Li, L.; Dong, Y.; Chen, G.; Shi, H. Remarkable photocatalytic activity enhancement of CO_2 conversion over 2D/2D g-C_3N_4/$BiVO_4$ Z-scheme heterojunction promoted by efficient interfacial charge transfer. *Carbon* **2020**, 160, 342-352.

(33) Xu, Q.; Zhu, B.; Jiang, C.; Cheng, B.; Yu, J. Constructing 2D/2D Fe_2O_3/g-C_3N_4 direct Z-scheme photocatalysts with enhanced H_2 generation performance. *Solar RRL* **2018**, 2, 1800006.

(34) You, Z.; Wu, C.; Shen, Q.; Yu, Y.; Chen, H.; Su, Y.; Wang, H.; Wu, C.; Zhang, F.; Yang, H. A novel efficient g-C_3N_4@BiOI p-n heterojunction photocatalyst constructed through the assembly of g-C_3N_4 nanoparticles. *Dalton Trans.* **2018**, 47, 7353-7361.

(35) Cai, T.; Zeng, W.; Liu, Y.; Wang, L.; Dong, W.; Chen, H.; Xia, X. A promising inorganic-organic Z-scheme photocatalyst Ag_3PO_4/PDI supermolecule with enhanced photoactivity and photostability for environmental remediation. *Appl. Catal. B Environ.* **2020**, 263, 118327.

(36) Guo, Y.; Li, J.; Gao, Z.; Zhu, X.; Liu, Y.; Wei, Z.; Zhao, W.; Sun, C. A simple and effective method for fabricating novel p-n heterojunction photocatalyst g-C_3N_4/$Bi_4Ti_3O_{12}$ and its photocatalytic performances. *Appl. Catal.*

DOI: 10.14102/j.cnki.0254-5861.2022-0188

B Environ. **2016**, 192, 57-71.
(37) You, Y.; Wang, S.; Xiao, K.; Ma, T.; Zhang, Y.; Huang, H. Z-Scheme g-C_3N_4/Bi_4NbO_8Cl heterojunction for enhanced photocatalytic hydrogen production. *ACS Sustain. Chem. Eng.* **2018**, 6, 16219-16227.
(38) Zhang, X.; Xiao, J.; Peng, C.; Xiang, Y.; Chen, H. Enhanced photocatalytic hydrogen production over conjugated polymer/black TiO_2 hybrid: the impact of constructing active defect states. *Appl. Surf. Sci.* **2019**, 465, 288-296.
(39) Xia, P.; Zhu, B.; Cheng, B.; Yu, J.; Xu, J. 2D/2D g-C_3N_4/MnO_2 nanocomposite as a direct Z-scheme photocatalyst for enhanced photocatalytic activity. *ACS Sustain. Chem. Eng.* **2018**, 6, 965-973.
(40) Yu, F.; Wang, Z.; Zhang, S.; Ye, H.; Kong, K.; Gong, X.; Hua, J.; Tian, H. Molecular engineering of donor-acceptor conjugated polymer/g-C_3N_4 heterostructures for significantly enhanced hydrogen evolution under visible-light irradiation. *Adv. Funct. Mater.* **2018**, 28, 1804512.
(41) Zhang, X.; Peng, B.; Zhang, S.; Peng, T. Robust wide visible-light-responsive photoactivity for H_2 production over a polymer/polymer heterojunction photocatalyst: the significance of sacrificial reagent. *ACS Sustain. Chem. Eng.* **2015**, 3, 1501-1509.
(42) Ke, X.; Dai, K.; Zhu, G.; Zhang, J.; Liang, C. *In situ* photochemical synthesis noble-metal-free NiS on CdS diethylenetriamine nanosheets for boosting photocatalytic H_2 production activity. *Appl. Surf. Sci.* **2019**, 481, 669-677.
(43) Sun, L.; Shi, Y.; Li, B.; Li, X.; Wang, Y. Preparation and characterization of polypyrrole/TiO_2 nanocomposites by reverse microemulsion polymerization and its photocatalytic activity for the degradation of methyl orange under natural light. *Polym. Compos.* **2013**, 34, 1076-1080.
(44) Jo, W.; Kang, H. (Ratios: 5, 10, 50, 100, and 200) polyaniline-TiO_2 composites under visible- or UV-light irradiation for decomposition of organic vapors. *Mater. Chem. Phys.* **2013**, 143, 247-255.
(45) Belabed, C.; Tab, A.; Moulai, F.; Černohorský, O.; Boudiaf, S.; Benrekaa, N.; Grym, J.; Trari, M. ZnO nanorods-PANI heterojunction dielectric, electrochemical properties, and photodegradation study of organic pollutant under solar light. *Int. J. Hydrogen Energy* **2021**, 46, 20893-20904.
(46) Zeng, W.; Cai, T.; Liu, Y.; Wang, L.; Dong, W.; Chen, H.; Xia, X. An artificial organic-inorganic Z-scheme photocatalyst WO_3@Cu@PDI supramolecular with excellent visible light absorption and photocatalytic activity. *Chem. Eng. J.* **2020**, 381, 122691.
(47) Zhang, Q.; Zhou, S.; Fu, S.; Wang, X. Tetranitrophthalocyanine zinc/TiO_2 nanofibers organic-inorganic heterostructures with enhanced visible photocatalytic activity. *Nano* **2017**, 12, 1750117.
(48) Pei, K.; Zhai, T. Emerging 2D organic-inorganic heterojunctions. *Cell Rep. Phys. Sci.* **2020**, 1, 100166.
(49) Wang, H.; Qian, C.; Liu, J.; Zeng, Y.; Wang, D.; Zhou, W.; Gu, L.; Wu, H.; Liu, G.; Zhao, Y. Integrating suitable linkage of covalent organic frameworks into covalently bridged inorganic/organic hybrids toward efficient photocatalysis. *J. Am. Chem. Soc*. **2020**, 142, 4862-4871.
(50) Yan, J.; Wu, H.; Chen, H.; Zhang, Y.; Zhang, F.; Frank Liu, S. Fabrication of TiO_2/C_3N_4 heterostructure for enhanced photocatalytic Z-scheme overall water splitting. *Appl. Catal. B Environ.* **2016**, 191, 130-137.
(51) Cheng, C.; He, B.; Fan, J.; Cheng, B.; Cao, S.; Yu, J. An inorganic/organic S-scheme heterojunction H_2-production photocatalyst and its charge transfer mechanism. *Adv. Mater.* **2021**, 33, 2100317.
(52) Yuan, X.; Wang, C.; Dragoe, D.; Beaunier, P.; Colbeau-Justin, C.; Remita, H. Highly promoted photocatalytic hydrogen generation by multiple electron transfer pathways. *Appl. Catal. B Environ.* **2021**, 281, 119457.
(53) Dai, K.; Hu, T.; Zhang, J.; Lu, L. Carbon nanotube exfoliated porous reduced graphene oxide/CdS-diethylenetriamine heterojunction for efficient photocatalytic H_2 production. *Appl. Surf. Sci.* **2020**, 512, 144783.
(54) Xiang, Y.; Wang, X.; Zhang, X.; Hou, H.; Dai, K.; Huang, Q.; Chen, H. Enhanced visible light photocatalytic activity of TiO_2 assisted by organic semiconductors: a structure optimization strategy of conjugated polymers. *J. Mater. Chem. A* **2018**, 6, 153-159.
(55) Wang, J.; Fan, Y.; Pan, R.; Hao, Q.; Ye, J.; Wu, Y.; Ree, T. *In situ* bridging nanotwinned all-solid-state Z-scheme g-C_3N_4/$CdCO_3$/CdS heterojunction photocatalyst by metal oxide for H_2 evolution. *Nanoscale* **2022**, 14, 7408-7417.
(56) Kong, L.; Yan, J.; Li, P.; Frank Liu, S. Fe_2O_3/C-C_3N_4-based tight heterojunction for boosting visible-light-driven photocatalytic water oxidation. *ACS Sustain. Chem. Eng.* **2018**, 6, 10436-10444.
(57) Zhang, J.; Zhang, G.; Zhang, J. Organic/inorganic nitride heterostructure for efficient photocatalytic oxygen evolution. *Appl. Surf. Sci.* **2019**, 475, 256-263.
(58) Bai, Y.; Nakagawa, K.; Cowan, A.; Aitchison, C.; Yamaguchi, Y.; Zwijnenburg, M.; Kudo, A.; Sprick, R.; Cooper, A. Photocatalyst Z-scheme system composed of a linear conjugated polymer and $BiVO_4$ for overall water splitting under visible light. *J. Mater. Chem. A* **2020**, 8, 16283-16290.
(59) Zhao, G.; Huang, X.; Fina, F.; Zhang, G.; Irvine, J. Facile structure design based on C_3N_4 for mediator-free Z-scheme water splitting under visible light. *Catal. Sci. Technol.* **2015**, 5, 3416-3422.
(60) Pan, Z.; Zhang, G.; Wang, X. Polymeric carbon nitride/RGO/Fe_2O_3: all solid state Z-scheme system for photocatalytic overall water splitting. *Angew. Chem. Int. Ed.* **2019**, 58, 7102-7106.
(61) Jiang, Z.; Sun, H.; Wang, T.; Wang, B.; Wei, W.; Li, H.; Yuan, S.; An, T.; Zhao, H.; Yu, J.; Wong, P. Nature-based catalyst for visible-light-driven photocatalytic CO_2 reduction. *Energy Environ. Sci.* **2018**, 11, 2382-2389.
(62) Ran, J.; Jaroniec, M.; Qiao, S. Cocatalysts in semiconductor-based photocatalytic CO_2 reduction: achievements, challenges, and opportunities. *Adv. Mater* **2018**, 30, 1704649.
(63) Habisreutinger, S.; Schmidt-Mende, L.; Stolarczyk, J. Photocatalytic reduction of CO_2 on TiO_2 and other semiconductors. *Angew. Chem. Int. Ed.* **2013**, 52, 7372.
(64) Chang, X.; Wang, T.; Gong, J. CO_2 photo-reduction: insights into CO_2 activation and reaction on surfaces of photocatalysts. *Energy Environ. Sci.* **2016**, 9, 2177.
(65) Izumi, Y. Recent advances in the photocatalytic conversion of carbon dioxide to fuels with water and/or hydrogen using solar energy and beyond. *Coord. Chem. Rev.* **2013**, 257, 171.
(66) Wang, Y.; Zhao, Z.; Sun, R.; Bian, J.; Zhang, Z.; Jing, L. TiO_2-modulated tetra(4-carboxyphenyl)porphyrin/perylene diimide organic Z-scheme nano-heterojunctions for efficiently visible-light catalytic CO_2 reduction. *Nanoscale* **2022**, 14, 8041-8049.
(67) Guo, H.; Chen, M.; Zhong, Q.; Wang, Y.; Ma, W.; Ding, J. Synthesis of Z-scheme α-Fe_2O_3/g-C_3N_4 composite with enhanced visible-light photocatalytic reduction of CO_2 to CH_3OH. *J. CO_2 Util.* **2019**, 33, 233-241.
(68) Jiang, Z.; Wan, W.; Li, H.; Yuan, S.; Zhao, H.; Wong, P. A hierarchical Z-scheme α-Fe_2O_3/g-C_3N_4 hybrid for enhanced photocatalytic CO_2 reduction. *Adv. Mater*. **2018**, 30 1706108.
(69) Zhang, L.; Wang, W.; Wang, H.; Ma, X.; Bian, Z. Design of inorganic-organic hybrid photocatalytic systems for enhanced CO_2 reduction under visible light. *Chem. Eng. Sci*. **2019**, 207, 1246-1255.
(70) Dong, W.; Jia, J.; Wang, Y.; An, J.; Yang, O.; Gao, X.; Liu, Y.; Zhao,

DOI: 10.14102/j.cnki.0254-5861.2022-0188

J.; Li, D. Visible-light-driven solvent-free photocatalytic CO_2 reduction to CO by Co-MOF/Cu_2O heterojunction with superior selectivity. *Chem. Eng. J*. **2022**, 438, 135622.

(71) Di, T.; Zhu, B.; Cheng, B.; Yu, J.; Xu, J. A direct Z-scheme g-C_3N_4/SnS_2 photocatalyst with superior visible-light CO_2 reduction performance. *J. Catal.* **2017**, 352, 532-541.

(72) Ohno, T.; Murakami, N.; Koyanagi, T.; Yang, Y. Photocatalytic reduction of CO_2 over a hybrid photocatalyst composed of WO_3 and graphitic carbon nitride (g-C_3N_4) under visible light. *J. CO_2 Util.* **2014**, 6, 17-25.

(73) Yu, W.; Xu, D.; Peng, T. Enhanced photocatalytic activity of g-C_3N_4 for selective CO_2 reduction to CH_3OH via facile coupling of ZnO: a direct Z-scheme mechanism. *J. Mater. Chem. A* **2015**, 3, 19936-19947.

(74) Murugesan, P.; Narayanan, S.; Manickam, M.; Murugesan, P.; Subbiah, R. A direct Z-scheme plasmonic AgCl@g-C_3N_4 heterojunction photocatalyst with superior visible light CO_2 reduction in aqueous medium. *Appl. Surf. Sci*. **2018**, 450, 516-526.

(75) Guo, H.; Wan, S.; Wang, Y.; Ma, W.; Zhong, Q.; Ding, J. Enhanced photocatalytic CO_2 reduction over direct Z-scheme $NiTiO_3$/g-C_3N_4 nanocomposite promoted by efficient interfacial charge transfer. *Chem. Eng. J*. **2021**, 412, 128646.

(76) Liang, M.; Borjigin, T.; Zhang, Y.; Liu, H.; Liu, B.; Guo, H. Z-scheme Au@void@g-C_3N_4/SnS yolk-shell heterostructures for superior photocatalytic CO_2 reduction under visible light. *ACS Appl. Mater. Interfaces* **2018**, 10, 34123-34131.

(77) Wang, Y.; Hu, G.; Feng, Y.; Zhang, X.; Song, C.; Lin, J.; Huang, Y.; Zhang, Y.; Liu, Z.; Tang, C.; Yu, C. Formation of p-BN@Zn/Co-ZIF hybrid materials for improved photocatalytic CO_2 reduction by H_2O. *Mater. Res. Bull*. **2022**, 152, 11186.

(78) Wang, B.; Zhao, J.; Chen, H.; Weng, Y.; Tang, H.; Chen, Z.; Zhu, W.; She, Y.; Xia, J.; Li, H. Unique Z-scheme carbonized polymer dots/ $Bi_4O_5Br_2$ hybrids for efficiently boosting photocatalytic CO_2 reduction. *Appl. Catal. B Environ.* **2021**, 293, 120182.

(79) He, Y.; Zhang, L.; Fan, M.; Wang, X.; Walbridge, M.; Nong, Q.; Wu, Y.; Zhao, L. Z-scheme SnO_{2-x}/g-C_3N_4 composite as an efficient photocatalyst for dye degradation and photocatalytic CO_2 reduction. *Sol. Energy Mater. Sol. Cells* **2015**, 137, 175-184.

(80) Truong, Q.; Liu, J.; Chung, C.; Ling, Y. Photocatalytic reduction of CO_2 on $FeTiO_3$/TiO_2 photocatalyst. *Catal. Commun*. **2012**, 19, 85-89.

(81) He, Y.; Zhang, L.; Teng, B.; Fan, M. New application of Z-scheme Ag_3PO_4/g-C_3N_4 composite in converting CO_2 to fuel. *Environ. Sci. Technol.* **2015**, 49, 649-656.

(82) Li, M.; Zhang, L.; Wu, M.; Du, Y.; Fan, X.; Wang, M.; Zhang, L.; Kong, Q.; Shi, J. Mesostructured CeO_2/g-C_3N_4 nanocomposites: remarkably enhanced photocatalytic activity for CO_2 reduction by mutual component activations. *Nano Energy* **2016**, 19, 145-155.

(83) Chen, X.; Xu, Y.; Ma, X.; Zhu, Y. Large dipole moment induced efficient bismuth chromate photocatalysts for wide-spectrum driven water oxidation and complete mineralization of pollutants. *Natl. Sci. Rev.* **2020**, 7, 652-659.

(84) Zhang, Y.; Qin, H.; Hong, N.; Bao, L.; Wu, B. Syntheses, structures and photocatalytic degradation properties of two copper(II) coordination polymers with flexible bis(imidazole) ligand. *Chin. J. Struct. Chem.* **2021**, 40, 595-602.

(85) Gómez-Pacheco, C.; Sánchez-Polo, M.; Rivera-Utrilla, J.; López-Peñalver, J. Tetracycline removal from waters by integrated technologies based on ozonation and biodegradation. *Chem. Eng. J.* **2011**, 178, 115-121.

(86) Zhu, B.; Xia, P.; Li, Y.; Ho, W.; Yu, J. Fabrication and photocatalytic activity enhanced mechanism of direct Z-scheme g-C_3N_4/Ag_2WO_4 photocatalyst. *Appl. Surf. Sci.* **2017**, 391, 175-183.

(87) Xiong, J.; Li, X.; Huang, J.; Gao, X.; Chen, Z.; Liu, J.; Li, H.; Kang, B.; Yao, W.; Zhu, Y. CN/rGO@BPQDs high-low junctions with stretching spatial charge separation ability for photocatalytic degradation and H_2O_2 production. *Appl. Catal. B Environ.* **2020**, 5, 118602.

(88) Guo, F.; Shi, W.; Wang, H.; Han, M.; Li, H.; Huang, H.; Liu, Y.; Kang, Z. Facile fabrication of a CoO/g-C_3N_4 p-n heterojunction with enhanced photocatalytic activity and stability for tetracycline degradation under visible light. *Catal. Sci. & Tech.* **2017**, 7, 3325-3331.

(89) Geng, Y.; Chen, D.; Li, N.; Xu, Q.; Li, H.; He, J.; Lu, J. Z-Scheme 2D/2D α-Fe_2O_3/g-C_3N_4 heterojunction for photocatalytic oxidation of nitric oxide. *Appl. Catal. B Environ.* **2021**, 280, 119409.

(90) Hong, Y.; Li, C.; Zhang, G.; Meng, Y.; Yin, B.; Zhao, Y.; Shi, W. Efficient and stable Nb_2O_5 modified g-C_3N_4 photocatalyst for removal of antibiotic pollutant. *Chem. Eng. J.* **2016**, 299, 74-84.

(91) Gao, X.; Gao, K.; Li, X.; Shang, Y.; Fu, F. Hybrid PDI/BiOCl heterojunction with enhanced interfacial charge transfer for a full-spectrum photocatalytic degradation of pollutants. *Catal. Sci. Technol.* **2020**, 10, 372-381.

(92) Dai, B.; Zhao, W.; Wei, W.; Cao, J.; Yang, G.; Li, S.; Sun, C.; Leung, D. Photocatalytic reduction of CO_2 and degradation of bisphenol-S by g-C_3N_4/Cu_2O@Cu S-scheme heterojunction: study on the photocatalytic performance and mechanism insight. *Carbon* **2022**, 193, 272-284.

(93) Chen, M.; Guo, C.; Hou, S.; Lv, J.; Zhang, Y.; Zhang, H.; Xu, J. A novel Z-scheme AgBr/P-g-C_3N_4 heterojunction photocatalyst: excellent photocatalytic performance and photocatalytic mechanism for ephedrine degradation. *Appl. Catal. B Environ.* **2020**, 266, 118614.

(94) Yin, N.; Chen, H.; Yuan, X.; Zhang, Y.; Zhang, M.; Guo, J.; Zhang, Y.; Qiao, L.; Liu, M.; Song, K. Highly efficient photocatalytic degradation of norfloxacin via $Bi_2Sn_2O_7$/PDIH Z-scheme heterojunction: influence and mechanism. *J. Hazard. Mater*. **2022**, 436, 129317.

(95) Huang, W.; Shen, Z.; Cheng, J.-Z.; Liu, L.-L.; Yang, K.; Wen, H.-R.; Liu, S.-Y. C-H activation derived CPPs for photocatalytic hydrogen production excellently accelerated by a DMF cosolvent. *J. Mater. Chem. A* **2019**, 7, 24222-24230.

(96) Tan, Z.-R.; Xing, Y.-Q.; Cheng, J.-Z.; Zhang, G.; Shen, Z.-Q.; Zhang, Y.-J.; Liao, G.; Chen, L.; Liu, S.-Y. EDOT-based conjugated polymers accessed via C-H direct arylation for efficient photocatalytic hydrogen production. *Chem. Sci.* **2022**, 13, 1725-1733.

(97) Shen, Z.-Q.; Xing, Y.-Q.; Chen, Y.; Zhang, G.; Chen, L.; Liu, S.-Y. Nanoporous and nonporous conjugated donor-acceptor polymer semiconductors for photocatalytic hydrogen production. *Beilstein J. Nanotechnol.* **2021**, 12, 607-623.

Received: August 20, 2022
Accepted: September 11, 2022
Published online: September 20, 2022
Published: September 22, 2022

DOI: 10.14102/j.cnki.0254-5861.2022-0188

Yu-Qin Xing received her Master degree in Chemical Engineering from Jiangxi University of Science and Technology in 2022. Her research interests focus on photocatalytic water splitting using heterojunctions.

Shi-Yong Liu is a full professor at Jiangxi University of Science and Technology (JXUST). He received his B.S. degree from Nanchang University in 1999, his Master degree in 2005 from Fuzhou University, and his Ph.D. degree in 2008 from Zhejiang University (ZJU). He was postdoctoral researcher in 2010-2016 at ZJU, and a visiting professor in 2014-2015 and University of Washington, USA. He became a research scientist in 2008 at Taizhou University (Zhejiang) and joined JXUST in 2017. His research interests focus on the design and synthesis of organic semiconductor for renewable energy applications, such as photocatalysis and organic photovoltaics.

DOI: 10.14102/j.cnki.0254-5861.2022-0188